Variable Phytoplankton Iron Quotas Modify Marine Biogeochemistry and Dampen the Response to Varying Atmospheric Iron Deposition

N. A. Wiseman[1], J. K. Moore[1], B. S. Twining[2], D. S. Hamilton[3], and N. M. Mahowald[3]

[1]Dept. of Earth System Science, University of California Irvine, Irvine, CA.

[2]Bigelow Laboratory for Ocean Sciences, East Boothbay, ME.

[3]Department of Earth and Atmospheric Science, Cornell University, Ithaca, NY, USA.

Corresponding author: Nicola Wiseman (wisemann@uci.edu)

Key Points:

- It is necessary to include variable phytoplankton iron quotas in order to properly simulate the oceanic iron, carbon and nitrogen cycles
- Pyrogenic iron is a key soluble iron source and has first order impacts on the marine nitrogen inventory and therefore carbon cycling

Abstract

Dissolved iron (dFe) plays an important role in regulating marine biological productivity. In high nutrient, low chlorophyll (HNLC) regions (> 33% of the global ocean) iron is the primary growth limiting nutrient, and elsewhere can regulate nitrogen fixation and growth by diazotrophs. Overall, dFe supply potentially impacts half of global ocean productivity. The link between iron availability and carbon export is strongly dependent on the phytoplankton iron quotas, or cellular Fe:C ratios. This ratio can vary by more than an order of magnitude in the open ocean and is positively correlated with ambient dFe concentration in sparse field observations. The Community Earth System Model (CESM) ocean component has been modified to simulate dynamic, group-specific, phytoplankton iron quotas (Fe:C) that vary as a function of ambient iron concentration. The simulated Fe:C ratios match the spatial trends in the observations and improve the correlation with global-scale, observed nutrient distributions. Acclimation of phytoplankton Fe:C ratios dampens the biogeochemical response to varying atmospheric deposition fluxes of soluble iron, compared to a model with fixed Fe:C. However, varying atmospheric soluble iron supply still has first order impacts on global carbon and nitrogen fluxes, and on the spatial patterns of nutrient limitation; both of which are strongly sensitive to changes in pyrogenic sources of iron. Accounting for dynamic, phytoplankton iron quotas is critical for capturing the ocean biogeochemical responses to varying atmospheric soluble iron inputs, including expected changes in both the mineral dust and pyrogenic sources with climate warming and anthropogenic activity.

1 Introduction

Ocean biogeochemistry plays a key role in the global carbon cycle through uptake of atmospheric carbon dioxide (CO_2) and its long-term storage via the biological and solubility pumps (Volk & Hoffert, 1985). Phytoplankton help drive the biological pump by taking up dissolved inorganic carbon (DIC) and nutrients and converting them to biomass via photosynthesis. Iron is a key micronutrient in this process as it limits phytoplankton growth in regions where other nutrients, such as nitrogen and phosphorus, are readily available (Boyd et al., 2007; J. K. Moore et al., 2004). These iron limiting nutrients are termed high nutrient, low chlorophyll (HNLC) regions and compose >33% of the surface ocean (C. M. Moore et al., 2013; J. K. Moore et al., 2002; Ustick et al., 2021).

The ratio of carbon to nutrients in exported organic matter has long been used to simplify biogeochemical cycles, where a fixed, extended Redfield ratio (C:N:P:Fe) is assumed (Bruland et

al., 1991; Redfield et al., 1963; Twining et al., 2015). This ratio helps determine the efficiency of biological export of carbon with respect to potentially growth-limiting nutrients. However, a wide range of Fe:C ratios have been observed in both sinking organic matter and *in situ* phytoplankton cells, complicating our understanding of the interactions between iron and carbon biogeochemistry (Fung et al., 2000; King et al., 2012).

Initial measurements of phytoplankton iron quotas relied on either radioisotope uptake experiments or bulk, size fractionation measurements using graphite furnace atomic absorption spectrometry (GFAAS) and more recently, inductively-coupled plasma mass spectrometry (ICPMS) (Ho et al., 2003; Martin & Knauer, 1973; Schmidt & Hutchins, 1999; Sunda & Huntsman, 1995). However, these types of measurements each have some limitations. Radioisotope uptake experiments derive cellular Fe:C from uptake rates, which may not be representative of the biogenic quotas, while bulk size fractionation analysis via GFAAS and ICPMS relies on measurements of the entire size class, which may be skewed by mineral and detrital particles (King et al., 2012). These methods were also unable to detect low cellular iron concentrations due to detection limits and were unable to provide information on individual taxa versus entire community assemblages (Twining et al., 2003). Single-cell synchrotron x-ray fluorescence (SXRF) is a relatively newer method where individual cells are isolated and individually measured for their iron and phosphorus reservoirs, while cellular carbon is estimated from cell volume (Twining et al., 2003, 2015).

Fe:C uptake by phytoplankton is primarily controlled by dFe availability in HNLC regions where nitrogen and phosphorus are replete (Sunda & Huntsman, 1995). Measurements of individual taxa iron requirements have found high variation between groups, where coastal species can vary more than 100 fold while open ocean species vary by about a factor of 20 (Marchetti & Maldonado, 2016; Sunda et al., 1991). Coastal phytoplankton continue to accumulate iron under iron replete conditions -- up to 70 times higher than is needed to reach their maximum growth rate, suggesting that they are capable of luxury storage (Sunda & Huntsman, 1995; Twining et al., 2021). Differences in uptake rates between species were largely attributed to variations in cell surface area, where uptake rate is a function of the surface area to volume ratio and therefore smaller cells are more efficient at iron uptake due to the diffusive limitation of transport (Hudson & Morel, 1990; Morel et al., 1991; Sunda & Huntsman, 1995; Twining et al., 2004). Smaller cells such as *E. huxleyi* and prokaryotes such as cyanobacteria may also use siderophores in order to

increase their iron uptake, potentially leading to higher Fe:C ratios than larger eukaryotes in low-Fe settings (Sunda & Huntsman, 1995; Twining et al., 2004). Some variation in iron requirements between taxa has also been attributed to the specialized needs of certain groups. For example, nitrogen fixers such as *Trichodesmium* need iron for the nitrogenase enzyme that is required in order to reduce dinitrogen, and have been found to contain highly variable iron quotas, with Fe:C ratios ranging from 22-480 μmol Fe/mol C (Berman-Frank et al., 2001; Howard & Rees, 1996; Sañudo-Wilhelmy et al., 2001). Phytoplankton community composition can strongly influence the strength of the biological pump, as different phytoplankton groups dominate under different conditions and have varying export efficiencies (Buesseler, 1998; Hamilton, Moore, et al., 2020). It is therefore important to accurately represent both the community composition as well as the nutrient requirements of the community in order to understand ocean carbon cycling.

Limited field observations have shown that phytoplankton Fe:C is generally elevated in regions of higher iron concentrations. In the North Atlantic subtropical gyre, under the North African dust plume transport pathway, phytoplankton Fe:C can reach upwards of 90 μmol/mol (Twining et al., 2015). Ratios also tend to be higher in coastal regions, where there is a significant continental shelf iron source due to shallower depths. These ratios tend to be lower in more remote regions that have lower atmospheric iron inputs, such as in the Indian subtropical gyre and the Southern Ocean, where ratios tend to be in the 3-15 μmol/mol range (Hopkinson et al., 2013; Twining et al., 2019).

Using fixed Redfield values for the C:N and C:P of phytoplankton in ocean models has been found to underestimate carbon fluxes or overestimate nutrient fluxes, especially in oligotrophic, strongly nutrient limited regions (Buchanan et al., 2018; Galbraith & Martiny, 2015; Kwiatkowski et al., 2018; Moreno et al., 2018; Schneider et al., 2004; Tanioka & Matsumoto, 2017; Weber & Deutsch, 2012). As of the CMIP6 experiments, half of the models account for variable Fe:C ratios while the other half assume fixed stoichiometry (Séférian et al., 2020). Few studies have investigated the impacts of variable iron stoichiometry in long term climate scenarios. Recent work found that the linking of the iron and carbon cycles via biological Fe:C is key to controlling nutrient limitation patterns in the future ocean, with direct impacts on net primary productivity (Tagliabue et al., 2020). It may be necessary to include variable iron ratios in these models to accurately predict the biogeochemical responses to future climate change.

The primary sources of iron to the oceans are from atmospheric deposition, terrestrial runoff and rivers, continental shelf sediments, and hydrothermal vent systems (Tagliabue et al., 2017). In the subtropical and tropical oceans, atmospheric deposition tends to be the primary source of bioavailable iron, while in the polar regions the relative importance of continental shelf and hydrothermal vent dust increases (Tagliabue et al., 2017). Atmospheric iron deposition in particular may support more than 50% of the iron exported from the euphotic zone in many regions (Krishnamurthy et al., 2010). Variations in atmospheric iron input strongly impact spatial patterns of phytoplankton growth limitation and the areal extent of the high-nutrient, low-chlorophyll regions (Hamilton, Moore, et al., 2020; Krishnamurthy et al., 2010). This atmospheric iron deposition is composed of two primary components: desert mineral dust and pyrogenic aerosols (Hamilton, Scanza, et al., 2020; Mahowald et al., 2011). Only a fraction of the iron in the dust and pyrogenic aerosols is soluble upon deposition to the oceans. The solubility percentage of iron within desert mineral dust is highly uncertain, with estimates ranging from 1% to as high as 12%, with ocean biogeochemical models having previously often assumed a constant 1-2% solubility of the iron from dust sources (Archer & Johnson, 2000; Bopp et al., 2003; Fung et al., 2000; Jickells & Spokes, 2001; Lefèvre & Watson, 1999; Mahowald et al., 2009; Wu & Boyle, 2002). Conversely, iron from pyrogenic sourced aerosols is likely to be more soluble, and despite making up only a small fraction of the total deposition, could potentially present a significant portion of the total soluble iron deposition flux in the HNLC regions (Hamilton, Scanza, et al., 2020; Ito et al., 2019; Matsui et al., 2018; Sedwick et al., 2007). However, there are large uncertainties in constraining these pyrogenic sources in terms of their sources, differing physiochemical properties, and flux magnitudes, including that previous estimates of pyrogenic sourced iron may be significantly underestimated (Conway et al., 2019; Hamilton et al., 2022; Lamb et al., 2021; Liu et al., 2022). The FeMIP model intercomparison project has reported atmospheric iron deposition from dust over a wide range of 1.4-32.7 Gmol Fe yr^{-1} (Tagliabue et al., 2016). Recent atmospheric iron model intercomparison studies have shown that including this pyrogenic sourced iron is key to simulating observations of variations in iron solubility over the global ocean and that iron from a pyrogenic wildfire source stimulates the biological pump at a greater rate than iron from mineral dust (Hamilton, Scanza, et al., 2020; Ito et al., 2019, 2020; Myriokefalitakis et al., 2018). We conduct a series of simulations with the improved, dynamic Fe quota model to investigate the

biogeochemical impacts of variable atmospheric iron inputs and the relative importance of mineral dust and pyrogenic sources of iron.

2 Methods

We use the Community Earth System Model (CESM) ocean circulation, marine ecosystem and biogeochemistry components. The version used is modified from CESM v1.21, but includes most science modifications that were introduced in CESM v2.0, including variable phytoplankton phosphorus quotas and an explicit ligand, iron model (Long et al., 2021; Wang et al., 2019). The model contains three explicit phytoplankton groups: diatoms, nano- to pico-sized phytoplankton (a fraction of which is assigned an implicit calcifier group) and diazotrophs (Long et al., 2021; J. K. Moore et al., 2004). The model has one class of explicit, iron-binding ligands and external iron sources from atmospheric deposition (pyrogenic and mineral dust sourced iron), marine sediments, hydrothermal vents, and riverine inputs (Long et al., 2021; J. K. Moore & Braucher, 2008). We ran the simulations with constant pre-industrial CO_2 for 300 years and averaged the results over the last 20 years of the simulation.

The iron uptake rate and the Fe:C for new growth of these groups are a function of ambient iron concentration and a prescribed half-saturation constant, but vary only within a narrow range (2.5-6 μmol/mol for small phytoplankton and diatoms, and 14-48 μmol Fe/mol C for the diazotrophs (J. K. Moore et al., 2004). Here we test a much wider range of Fe:C ratios. The cellular iron to carbon ratio for new growth is assumed to be a linear function of the ambient dissolved iron concentration (Sunda & Huntsman, 1995). FeOpt is the group-specific, dissolved iron concentration where the Fe:C reaches its maximum value; above this concentration, the Fe:C for new growth is set at the prescribed maximum value (gQfe_max). When dissolved iron concentrations fall below FeOpt, the Fe:C for new growth decreases linearly with iron concentration until the prescribed minimum value is reached (gQfe_min) (Fig. 1).

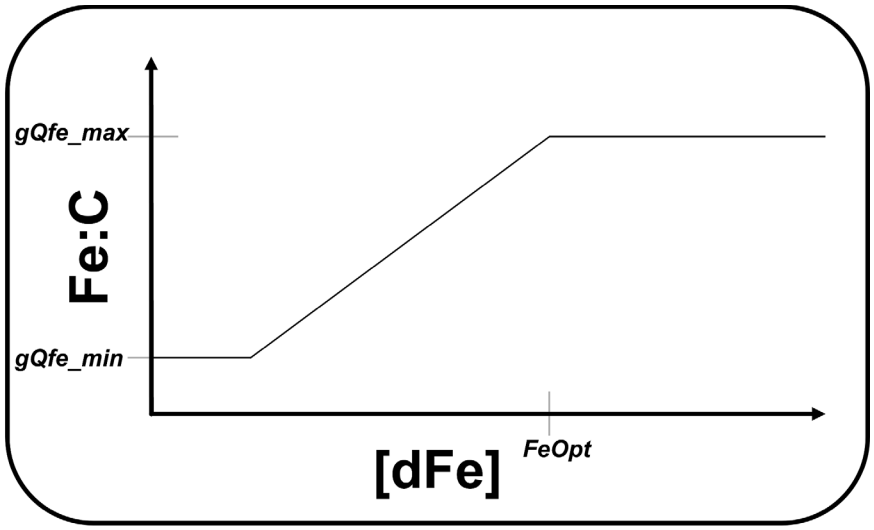

Figure 1. Phytoplankton Fe:C ratio for new growth as a function of dissolved iron. FeOpt determines the dissolved ambient iron concentration at which phytoplankton Fe:C reaches its maximum value (gQFe_max). Fe:C varies linearly with dissolved iron concentration between the prescribed, group-specific maximum (gQFe_max) and minimum (gQfe_min) quotas.

We test applying a broader range of Fe:C ratios, specific for each phytoplankton group, based on our compiled database of field observations (Table S1) of phytoplankton Fe:C where ambient dissolved iron was also measured (n = 142), including unpublished Arctic data from the Twining lab (Abraham et al., 2000; Hopkinson et al., 2013; King et al., 2012; Maldonado & Price, 1999; McKay et al., 2005; Sañudo-Wilhelmy et al., 2001; Sarthou et al., 2008; Schmidt & Hutchins, 1999; Tovar-Sanchez et al., 2003; Twining et al., 2004, 2010, 2011, 2015, 2019, 2021). These observations include bulk Fe:C as well as individual phytoplankton Fe:C for small phytoplankton, diatoms, and nitrogen fixers (Table S1 in supplemental materials (SM) for more details). Based on these observations, we test a range of maximum Fe:C ratios for new growth (gQFe_max) from 6.0 to 120 μmol Fe/mol C (12 - 240 μmol Fe/mol C for diazotrophs) as well as a range of FeOpt values from 1.0 nM to 2.0 nM for each phytoplankton group. We ended up with a final maximum gQFe_max of 90 μmol Fe/mol (180 μmol Fe/mol for diazotrophs) and an FeOpt of 1.75nM for all phytoplankton groups based on this tuning, where we aimed to best represent the observations of phytoplankton Fe quotas as well as observed global distributions of nutrients including iron, nitrogen, and phosphorus, nitrogen and phosphorus are from World Ocean Atlas (Garcia et al., 2019). Observational iron data is largely from the GEOTRACES project supplemented with historical data compilations (Anderson, 2020; J. K. Moore & Braucher, 2008; Tagliabue et al., 2012).

In order to investigate the impacts of variable plankton Fe:C stoichiometry on the coupling of the iron and carbon cycles, we compare simulations with the optimized variable Fe quota model with simulations using fixed Fe:C values of 3.0, 7.0, and 10.0 μmol Fe/mol C. We also compare variable versus fixed quotas in response to different levels of atmospheric iron deposition. We conduct a series of experiments with four different atmospheric iron deposition fields: pyrogenic Fe only, dust Fe only, dust + pyrogenic Fe, and dust Fe + pyrogenic Fe deposition where the solubility of the pyrogenic iron is doubled to account for uncertainties in the pyrogenic solubility (Hamilton, Scanza, et al., 2020). The dust deposition was extracted from the CMIP6 CESM2 historical simulation, averaged over the years 1990-2009 (Long et al., 2021). We assume the mineral dust is 3.5% iron by weight, and apply a spatially varying solubility for the aerosol iron at deposition. This solubility is a function of the ratio of coarser dust particle deposition / finer dust particle deposition in the CESM2 simulation, optimized to best match to surface iron observations (Long et al., 2021; J. K. Moore et al., in prep.). The ratio of coarse/fine dust at deposition is a useful proxy for the distance traveled from the mineral dust source regions, as the coarse dust particles are expected to be removed more quickly during atmospheric transport. The dust iron solubility ranges from 0.5% near dust source regions, gradually increasing to reach values of 10-14% in the remote central Pacific. The deposition of iron from pyrogenic sources includes soluble iron from wildfires and anthropogenic emissions with month to month seasonality. The deposition assumes a constant solubility in pyrogenic aerosols of 5%, which tends to be on the lower range of estimates, which is why we include the scenario where pyrogenic aerosols have a constant solubility of 10%, which is closer to estimates from the CAM6 model where wildfire sourced iron has a solubility of 18.8% and anthropogenic iron has a solubility of 11.2% (Hamilton, Moore, et al., 2020; Hamilton, Scanza, et al., 2020).

We force the ocean model with the pyrogenic soluble iron deposition combined with the soluble iron deposition from mineral dust in our optimal case. We include sensitivity experiments where we force the ocean model with only the pyrogenic-sourced iron and with only the dust-sourced iron. The global rate of soluble iron deposition for the pyrogenic and dust sources to the surface ocean is 1.5 Gmol Fe yr^{-1} and 4.0 Gmol Fe yr^{-1}, respectively, resulting in a total global deposition of 5.5 Gmol Fe yr^{-1}. A fourth sensitivity experiment combines the dust iron with the pyrogenic-sourced iron increased by a factor of two (7.0 Gmol Fe yr^{-1}), to account for uncertainties in the solubility and aerosol source strengths (Figure 2). One goal is to evaluate the importance of

the pyrogenic iron source in driving marine biogeochemistry. These experiments provide a wide range of estimates of the atmospheric deposition of soluble iron to the oceans (1.5 - 7.0 Gmol Fe yr^{-1}). Each experiment was performed with the optimal, variable Fe:C stoichiometry range of 3-90 µmol Fe /mol C (6-180 µmol Fe/mol C for the diazotrophs) as well as with fixed Fe:C stoichiometry at value of 7 µmol Fe /mol C, for comparison.

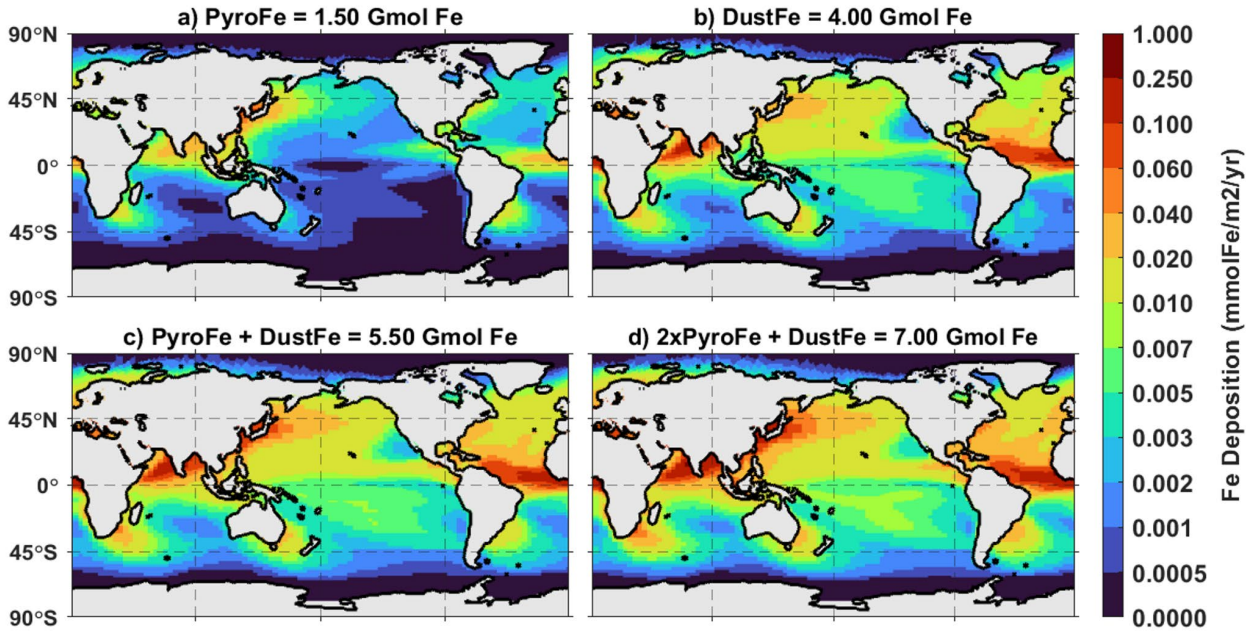

Figure 2. Atmospheric soluble iron deposition fields used to force the ocean biogeochemistry model. (a) PyroFe includes soluble iron from wildfires as well as fossil fuel combustion for an annual ocean surface deposition of 1.50 Gmol Fe. (b) DustFe includes soluble iron from lithogenic sources for an annual ocean surface deposition of 4.00 Gmol Fe. (c) Annual ocean surface soluble iron deposition from pyrogenic and lithogenic sources totaling 5.50 Gmol Fe. (d) Annual ocean surface soluble iron deposition from pyrogenic and lithogenic sources where the pyrogenic solubility is doubled for a total deposition of 7.00 Gmol Fe.

3 Results

We find that a broad Fe:C range for new growth (3-90 µmol Fe/mol C for the small phytoplankton and diatoms and a range of 6-180 µmol Fe/mol C for diazotrophs) best reproduces the patterns in field observations of phytoplankton Fe:C versus surface iron concentration, increasing the overall skill of the model (Fig. 3). CESM previously had varying Fe:C within a limited range of 2.5-6 µmol Fe/mol C for diatoms and small phytoplankton and 14-48 µmol/mol for diazotrophs (J. K. Moore et al., 2004). Each group has an optimal dFe concentration for growth

of 1.75 nM, so the maximum iron quotas are achieved only in the highest dFe surface concentration regions. The tuned model with these parameters is able to reproduce the observed relationship in observations of phytoplankton Fe:C and in situ dFe, where dissolved iron concentrations increase, so do the observed Fe:C ratios (Fig. 3a, R^2 of Fe:C vs dFe from observations, the tuned model, and the previous model were 0.77, 0.71, and 0.35, respectively). In the field observations, cellular Fe:C increases roughly linearly with dissolved iron variability on log-log plotting scale. The observed range of Fe:C ratios for small phytoplankton was 3-100 umol Fe/mol C and for diatoms was 4-528 (259) umol Fe/mol C (King et al., 2012; Twining et al., 2019).

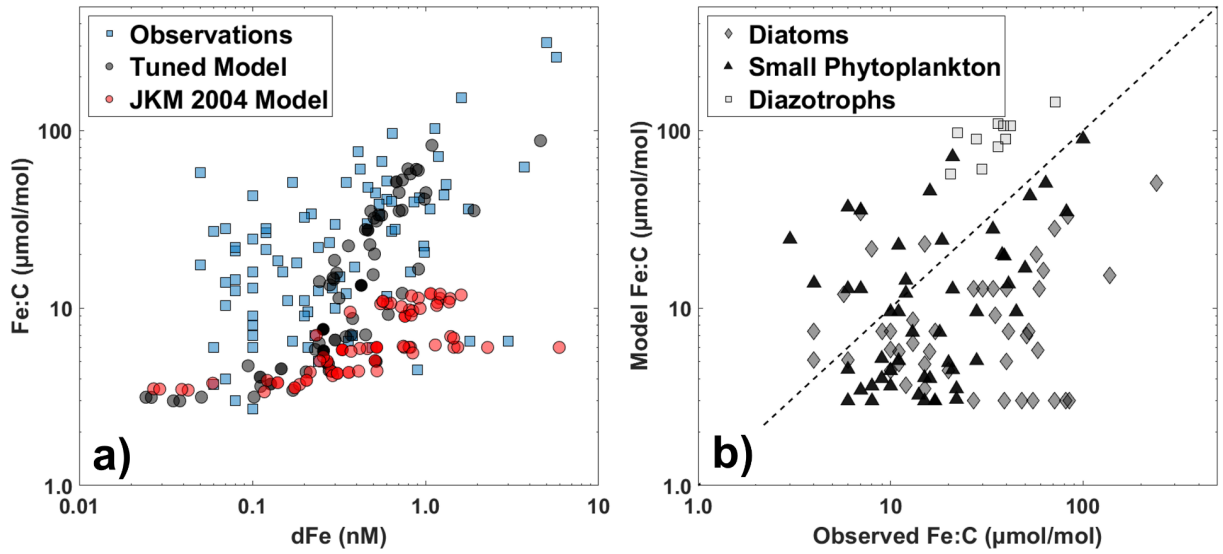

Figure 3. Comparison of field observations and simulation community average Fe:C of phytoplankton and dFe concentrations (a) and phytoplankton Fe:C in observations and simulations (b). Observed community Fe:C as a function of dFe (a, blue squares), tuned model Fe:C versus dFe (a, gray circles), previous model Fe:C versus dFe (a, red circles) extracted from the same locations as the field observation. Observations $R^2 = 0.77$, $p < 0.05$ (4e-18), tuned model $R^2 = 0.71$, $p < 0.05$ (6e-14), previous model $R^2 = 0.35$, $p < 0.05$ (1e-3). (b) Phytoplankton group specific model Fe:C versus observed phytoplankton Fe:C (gray diamonds are diatoms $R^2 = 0.83$, black triangles are small phyto $R^2 = 0.60$, white squares are diazotroph $R^2 = 0.81$). Model estimates were paired based on location and phytoplankton type. Dashed black line in (b) represents a 1:1 fit.

257 The model Fe:C also agrees with the individual cell iron to carbon measurements (Fig. 3b).
258 For each individual cell measurement we extracted model Fe:C for the same phytoplankton group
259 at the same location. Deviations from this fit tended to be regionally specific.

260 Overall, the model is able to reproduce the observed spatial variations in phytoplankton
261 Fe:C ratios (Fig. 4). Phytoplankton Fe:C is elevated in regions where surface dFe is elevated due
262 to regional inputs such high atmospheric dust deposition, coastal shelf sources, and upwelling.
263 Diazotroph Fe:C measurements are limited to the North Atlantic while small phytoplankton and
264 diatom measurements are available for most ocean basins. However, even within this small region
265 the model is able to replicate the gradient of decreasing Fe:C ratios for diazotrophs as dFe
266 decreases from coast to offshore. Regions where the model and observations tend to diverge may
267 be driven by colimitation. For example, the model underestimates diatom Fe:C in the oligotrophic
268 southern Pacific gyre, where recent studies have suggested nitrogen limitation may lead to
269 increases in the cellular Fe:C ratios (Twining et al., 2021). Using a limited range of Fe:C ratios
270 does not accurately capture the observed variation in Fe:C ratios. The R^2 values for model Fe:C
271 for each group (small phytoplankton, diatom, diazotrophs) versus observations were 0.83, 0.60,
272 and 0.81 respectively for the variable quota model, while they were 0.16, 0.32, and 0.34
273 respectively, with the original model with limited range in Fe:C.

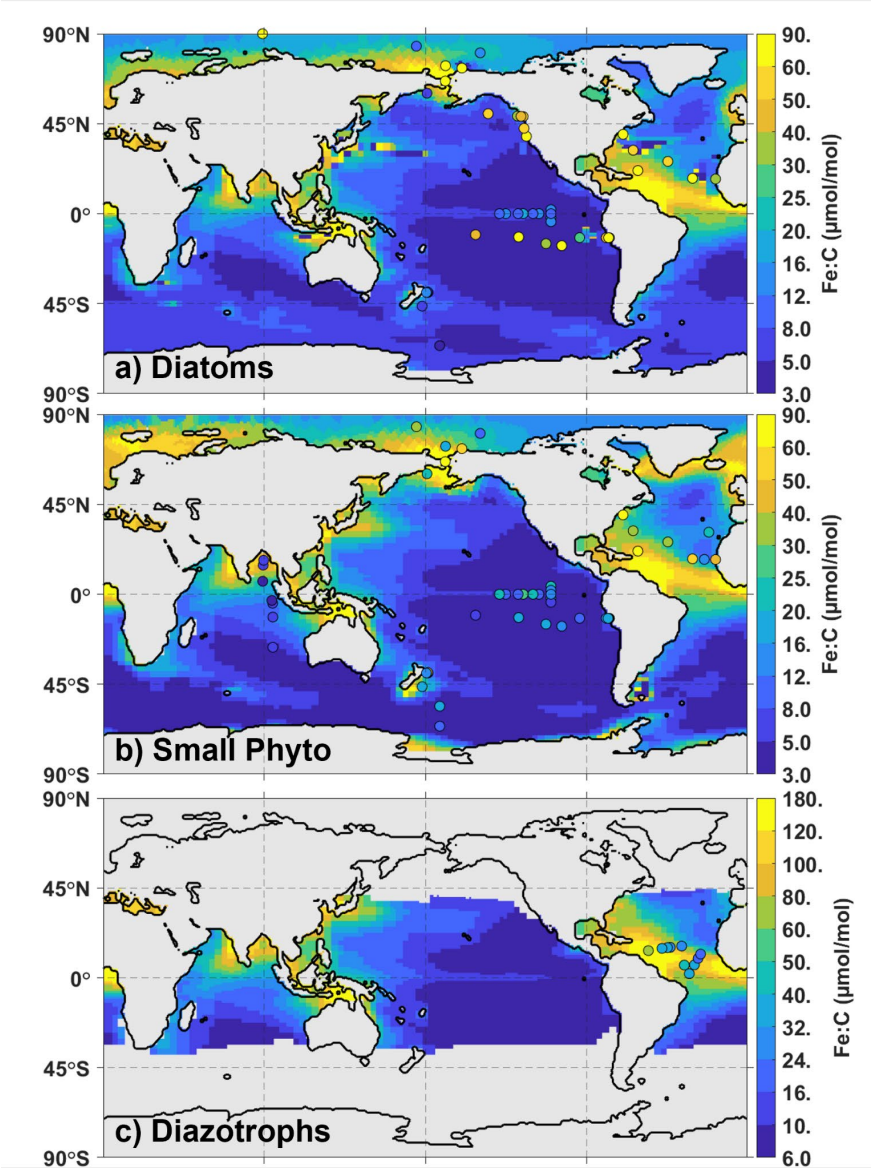

Figure 4. Optimized model patterns of (a) diatom group Fe:C overlaid with circles showing observations of diatom Fe:C ($R^2 = 0.83$), (b) small phytoplankton group Fe:C overlaid with circles showing observations of small phytoplankton Fe:C ($R^2 = 0.60$), and (c) diazotroph group Fe:C overlaid with circles showing observations of diazotroph Fe:C ($R^2 = 0.81$).

3.1 Fixed vs Variable Fe Quotas

We find that using fixed stoichiometry in place of variable stoichiometry has first order impacts on nutrient cycling within the surface ocean. One method that we use to quantify this impact is the HNLC index. We define an HNLC region in the Pacific Ocean between 25°N and 25°S, east of 150°E, and the HNLC index as the area in the HNLC region that has surface nitrate concentrations greater than 0.3 µM in the model output, divided by the same metric from the nitrate

from World Ocean Atlas 2018 (WOA18) (Garcia et al., 2019). With the expanded variable Fe:C range, we are able to reproduce the HNLC size as seen in the WOA18, with an HNLC index of 1.0063 (Fig. 5). With fixed stoichiometry however, the HNLC size is either overestimated or underestimated depending on the set fixed value. For fixed Fe:C ratios of 3, 7, and 10, the HNLC areal extent changes by -54%, +44%, and +81%, respectively (Fig 5).

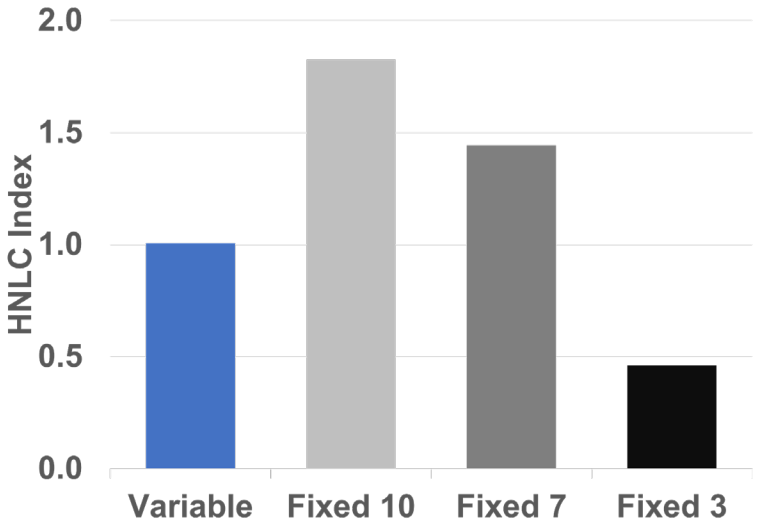

Figure 5. HNLC index for four simulations within the Central Pacific HNLC region (between 25°N and 25°S, east of 150°E). Index is defined as the ratio of ocean surface area where nitrate concentrations exceed 0.3 µM in each simulation compared to WOA18. Variable is the tuned model with variable Fe:C ranging from 3-90 µmol Fe/mol C for small phytoplankton and diatoms and 6-180 µmol Fe/mol C for diazotrophs, the fixed scenarios of 10, 7, and 3 are where the model phytoplankton Fe:C is fixed for all groups at 10, 7, and 3 µmol Fe/mol C, respectively.

Comparing the fixed ratios versus the optimized variable Fe quota model there are only modest impacts on carbon fluxes integrated at the global or Central Pacific HNLC region scale (Table 1). However, there are large shifts in the spatial patterns of NPP and carbon export across the simulations, with disproportionate impacts on key fluxes within the marine nitrogen cycle. Global NPP decreased by up to 5% with fixed quotas, and NPP in the HNLC region decreased by up to 9% (Table 1). The regional NPP response to the chosen fixed value for Fe:C is non-linear, with the fixed value of 7 µmol Fe/mol C having the weakest response of a 3% decrease, while the 3 and 10 µmol Fe/mol C versions had stronger decreases of 7% and 9%.

Table 1. Changes in key annual global and regional carbon fluxes in the optimal model when fixed stoichiometry is used versus the expanded variable range. Percentages are percent change from the tuned variable model where Fe:C ranges from 3-90 μmol Fe/mol C for small phytoplankton and diatoms and 6-180 μmol Fe/mol C for diazotrophs. The fixed scenarios of 10, 7, and 3 are where the model phytoplankton Fe:C is fixed for all groups at 10, 7, and 3 μmol Fe/mol C, respectively. NPP is net primary productivity, POC is particulate organic carbon, HNLC is Central Pacific high nutrient low chlorophyll region between 25°N and 25°S, east of 150°E.

Fe:C	NPP (PgC/yr)	POC Export (PgC/yr)	Nitrogen Fixation (TgN/yr)	Water Column Denitrification (TgN/yr)	HNLC NPP (PgC/yr)	HNLC POC Export (PgC/yr)
Variable	53.8	8.5	225.3	63.1	13.6	2.03
Fixed 10	51.2 (-5%)	8.0 (-6%)	173.1 (-23%)	20.6 (-67%)	12.4 (-9%)	1.74 (-14%)
Fixed 7	52.8 (-2%)	8.3 (-2%)	201.6 (-10%)	40.6 (-35%)	13.2 (-3%)	1.93 (-5%)
Fixed 3	53.3 (-1%)	8.6 (+2%)	260.6 (+15%)	102.4 (+62%)	12.7 (-7%)	1.94 (-4%)

Surface chlorophyll patterns shift sharply in the tropical Pacific in response to the treatment of plankton Fe quotas (Fig. 6). While the optimized model is able to reproduce patterns seen in satellite chlorophyll products ($r^2 = 0.48$), a fixed ratio of 10 μmol Fe/mol C results in up to 60% underestimation of surface chlorophyll in the equatorial upwelling zone, while the more western region of the Pacific sees overestimates of up to 60% in some regions. In contrast, using a fixed Fe:C ratio of 3 μmol Fe/mol C results in an overestimate of chlorophyll in the equatorial upwelling tongue by greater than 100%. This is due to the increase in iron availability from the lack of efficient iron export, leading to a buildup of available iron in the surface waters. This allows for phytoplankton to increase their biomass to a greater extent than they would under stronger iron limitation, thereby driving the increase in surface chlorophyll. However, due to the reduced iron limitation, the surrounding areas transition to nitrogen limitation, resulting in a decrease in surface chlorophyll outside of the equatorial upwelling tongue. The variable Fe quota model, which gives high Fe:C in the plankton near the coast and very low Fe:C values in the offshore waters, is best able to replicate the satellite chlorophyll patterns.

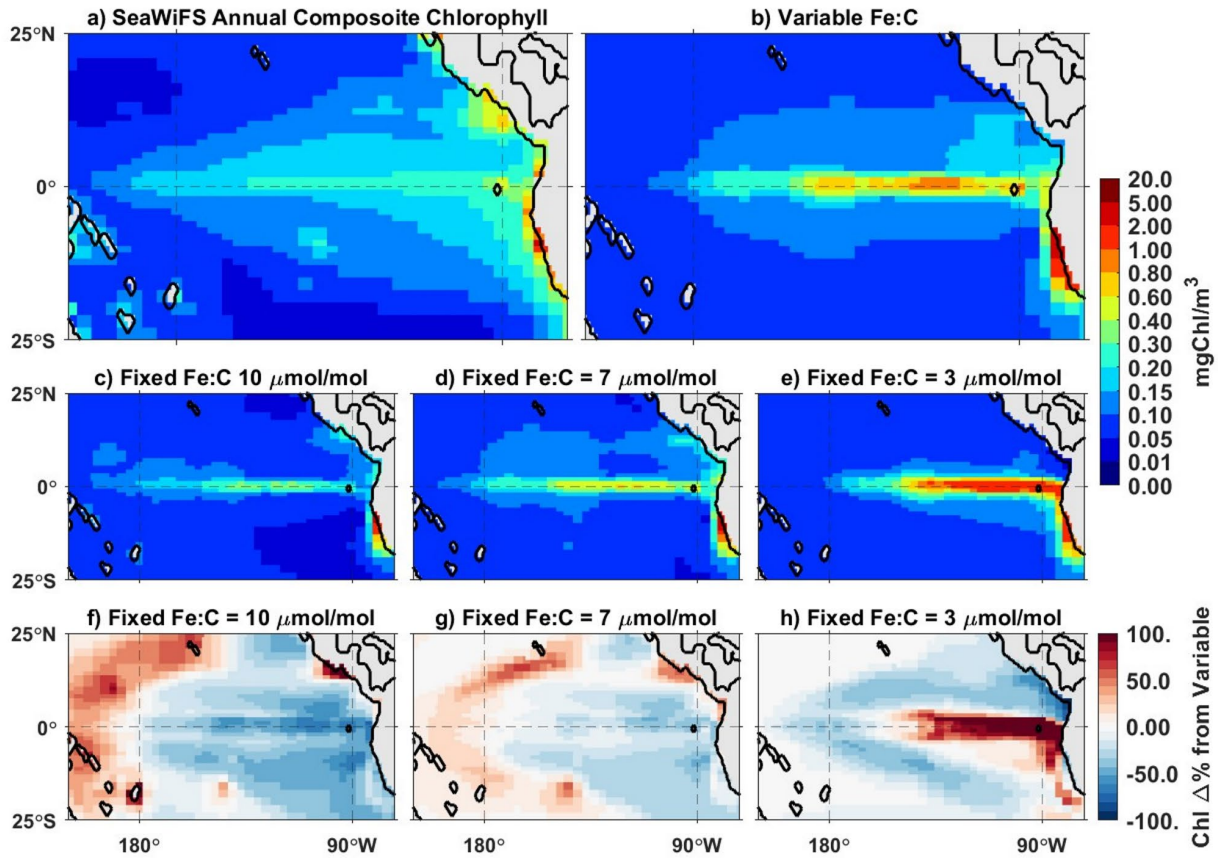

Figure 6. SeaWiFS chlorophyll climatology (a) and optimized model surface chlorophyll (b, mgChl/m^3) for our HNLC region. Middle panels show surface chlorophyll for fixed Fe:C simulations (c-e), bottom panels show the percent change of chlorophyll for fixed Fe:C simulations (f-h) compared to the dynamic iron quota model.

There are also large shifts in the spatial patterns of sinking particulate organic carbon (POC) export in this region (Fig. 7). The simulation with a fixed Fe:C of 7 µmol Fe/mol C had the pattern most similar to the variable quota model. In the 10 µmol Fe/mol C simulation most of the sediment-sourced iron is used up nearshore, with little advection to the open ocean (Fig 7c). In contrast, with the 3 µmol Fe/mol C quota, much less iron is used up nearshore, and there is a much larger lateral flux of iron to the open ocean. These shifts in the spatial patterns of export influence the amount of organic matter sinking into the oxygen minimum zones, leading to large swings in the rates of water column denitrification, even though the integrated, total POC export changes only modestly at the global or regional scales (Table 1).

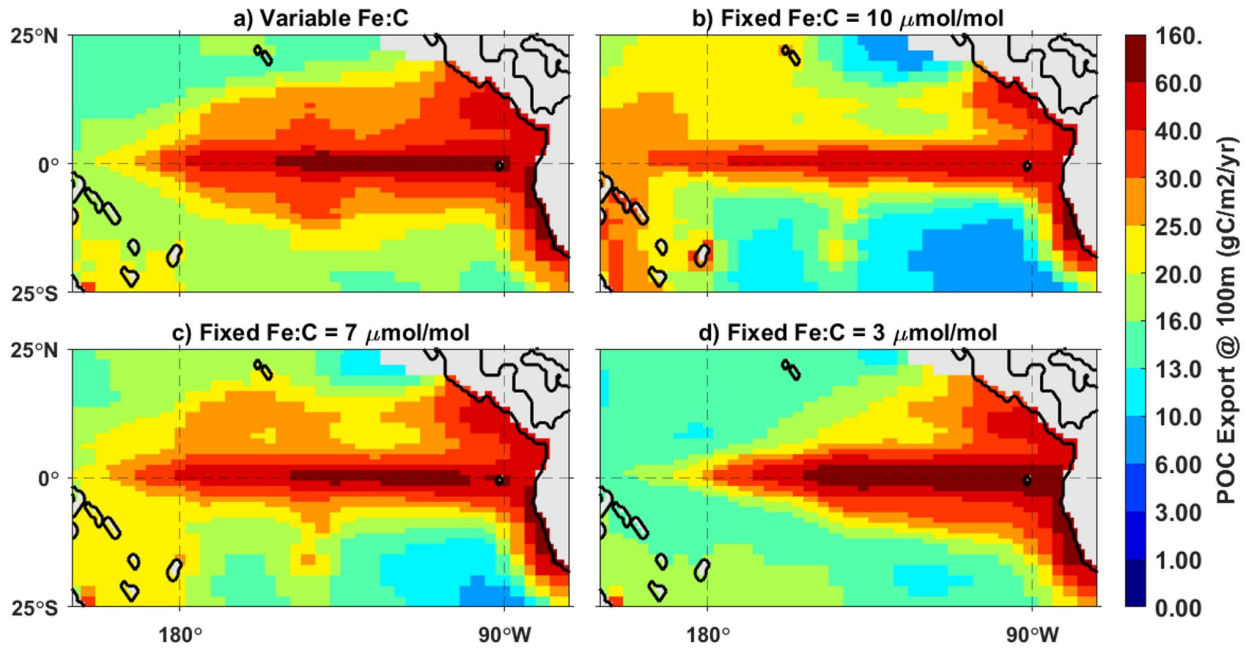

Figure 7. Sinking particulate organic carbon (POC) export at 100m depth comparing the dynamic Fe:C model (a) and with simulations using fixed Fe:C ratios of 3, 7, and 10 µmol Fe/mol C (b-d, respectively).

Varying plankton iron quotas changes the efficiency of the biological export of iron. This can have strong impacts on the spatial patterns of nutrient limitation as iron becomes exported more or less efficiently relative to the other nutrients. With a fixed Fe:C ratio of 7 µmol Fe/mol C, the iron-limited areas expand substantially, compared with the variable Fe:C simulation (Fig. 8). The iron-limited area for the small phytoplankton group increases from 37.4% of total ocean area with variable Fe:C, up to 45.5% and 56.78% with the fixed Fe:C of 7 and 10 µmol Fe/mol C respectively (Fig. 8). This is because iron is already limiting in the HNLC regions, and when higher Fe:C ratios are prescribed, iron is exported more efficiently per unit carbon, resulting in even less iron being available in the regions and therefore stronger iron limitation. With a fixed ratio of 3 µmol Fe/mol C, the HNLC region outside of the equatorial upwelling zone transitions from iron limitation to nitrogen limitation, as less iron is exported per mol of carbon and iron limitation is weakened. This results in the region transition to nitrogen limitation as nitrate supply is high here due to upwelling and can be readily consumed when iron is available due to the inefficient export..

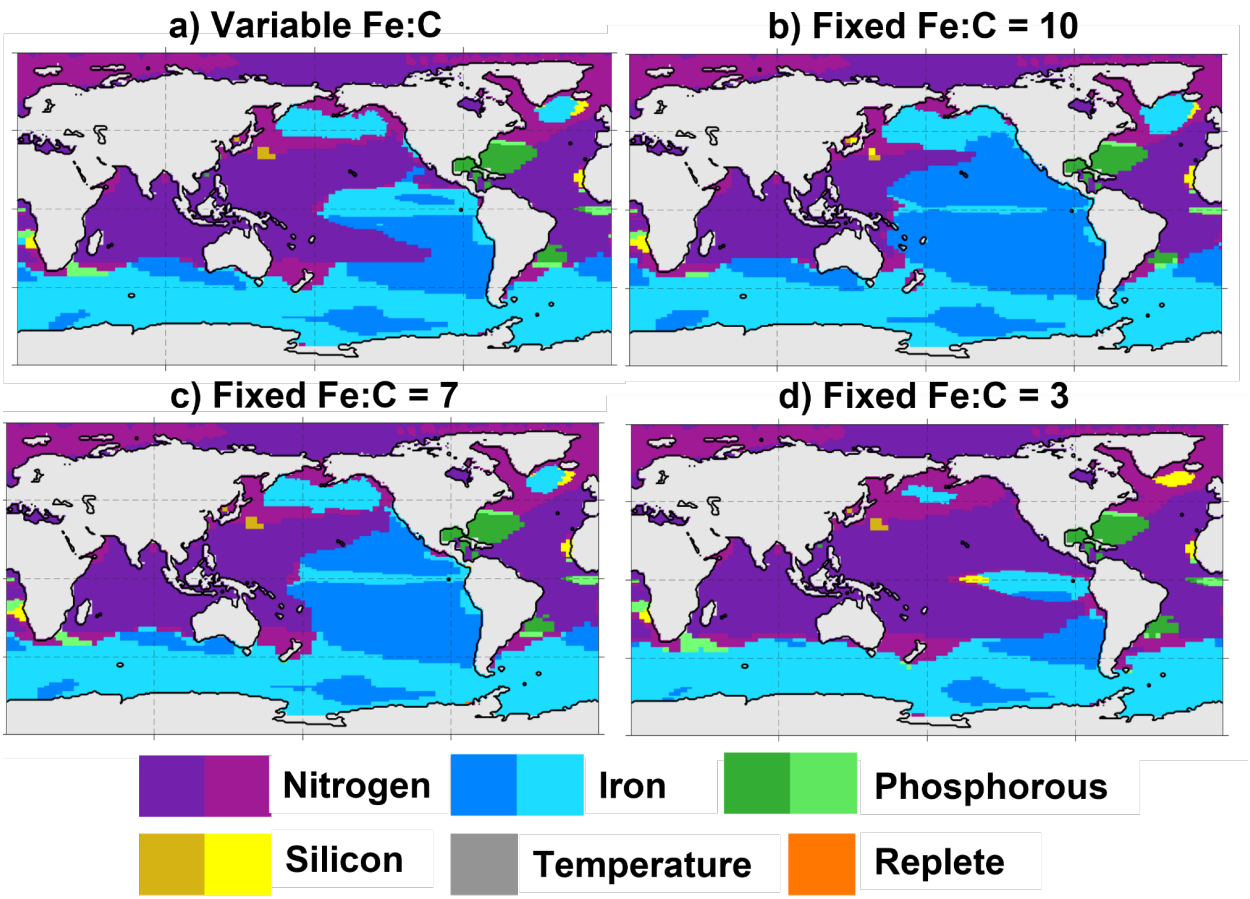

Figure 8. Patterns of nutrient limitation of diatom growth from variable and fixed iron quota simulations. Phytoplankton are nutrient replete when nutrient limitation reduces growth by less than 10%. Darker color shading indicates where growth is reduced by more than 50% from the maximum growth rate. The tuned model is shown in (a) and the simulations using fixed Fe:C ratios of 3, 7, and 10 µmol Fe/mol C are (b-d) respectively.

3.2 Impacts of Varying Iron Deposition on Ocean Biogeochemistry

Using fixed versus variable stoichiometry amplifies the impacts of changing iron deposition on the global ocean carbon cycle. At lower deposition rates, using fixed Fe:C has a larger impact on carbon cycling, with NPP 15% lower and sinking particulate organic carbon (POC) 51% lower when a fixed Fe:C of 10 µmol Fe/mol C is used versus the variable ratios (Table 2).

With increasing deposition, NPP and sinking POC do not respond as strongly when using fixed versus variable stoichiometry, with NPP and POC being 3% and 5% lower respectively (Table 1). There is a modest change in NPP from low deposition to high deposition (50.3-53.8 PgC/yr) when the optimal variable Fe:C is used. By having dynamic, variable iron quotas,

383 phytoplankton are able to partially dampen, or buffer, the effects of changing iron deposition by
384 decreasing Fe:C when iron is scarce to maintain productivity. Increasing Fe:C ratios lead to more
385 efficient export of iron with increasing iron deposition. Thus, models with fixed Fe quotas will
386 overestimate the biogeochemical impacts of varying iron deposition, by not accounting for this
387 phytoplankton acclimation to available nutrient concentrations.
388
389 **Table 2.** Percent change in key carbon fluxes for the pyrogenic iron scenarios compared to the
390 optimal deposition scenario with variable stoichiometry.

Deposition	Fe:C	Global NPP	Global POC Export	HNLC NPP	HNLC POC Export
CESM2opt	Variable	53.8 PgC	8.5 PgC	13.6 PgC	2.03 PgC
5.5 Gmol Fe/yr					
PyroFe	Variable	-7%	-9%	-15%	-21%
1.5 Gmol Fe/yr	Fixed 7	-13%	-14%	-32%	-37%
DustFe	Variable	+0.2%	-1%	+2%	+0.3%
4.0 Gmol Fe/yr	Fixed 7	-3%	-4%	-4%	-8%
DustFe + 2xPyroFe	Variable	-0.4%	+1%	-2%	-1%
7.0 Gmol Fe/yr	Fixed 7	-2%	-1%	-3%	-4%

391

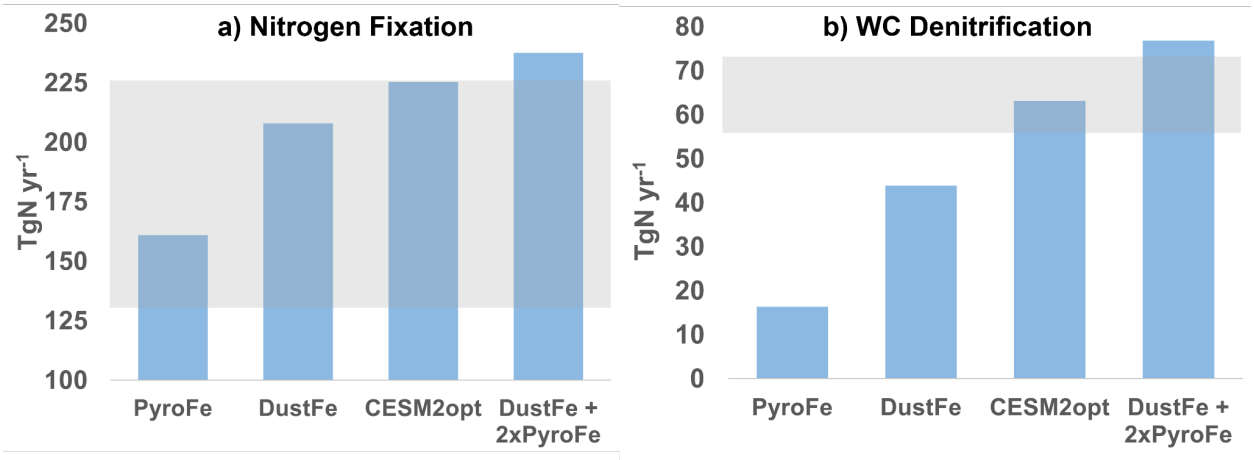

392

393 **Figure 9.** Global annual nitrogen fixation (a) and water column denitrification (b) under the
394 various iron deposition scenarios. The gray boxes represent the estimated ranges for nitrogen
395 fixation and water column denitrification from a recent inverse model study (Wang et al., 2019).

The variations in atmospheric iron inputs have strong impacts on some key global nitrogen fluxes in conjunction with the optimized variable Fe quota model. When atmospheric deposition is decreased, (PyroFe and DustFe simulations), both nitrogen fixation and water column denitrification decrease drastically. The reduction in nitrogen fixation can be attributed to the decrease in diazotroph productivity. Diazotrophs are iron limited in much of the surface ocean. Therefore, when the atmospheric deposition is decreased, their productivity is reduced, and global rates of nitrogen fixation decrease accordingly. The decrease in water column denitrification can be attributed to a general decrease in productivity and therefore carbon export, especially in the eastern Pacific, where iron is the primary limiting nutrient. This impacts the HNLC regions in particular, which increase in area by 23% when pyrogenic sourced iron is omitted, where iron limitation expands to regions that were previously nitrogen limited. With the reduction of atmospheric iron deposition and stronger iron limitation, primary productivity decreases, resulting in less organic matter sinking through the oxygen deficient zones. With less organic matter to degrade, water column denitrification drops dramatically. This feedback between iron limitation and water column denitrification is one of the key links between the iron and nitrogen cycles. Proper estimates of iron deposition are necessary in order to accurately simulate the global marine nitrogen cycle. When the optimal iron deposition field is used, the simulated global nitrogen fixation rate is 225 TgN yr^{-1}, while the global water column denitrification rate is 63 TgN yr^{-1}, which are both in agreement with recent inverse model estimates (Wang et al., 2019).

4 Conclusions

Phytoplankton Fe:C uptake links not only the oceanic iron and carbon cycles, but the nitrogen cycle as well. It is therefore necessary that phytoplankton iron quotas represent the observed biological patterns. This requires not only variable quotas, but also a high variable range to best represent the flexibility of these phytoplankton groups under a changing environment. We find that a range of 3-90 μmol Fe/mol C for the small phytoplankton and diatoms and a range of 6-180 μmol Fe/mol C for diazotrophs best represents not only field observations of individual cell iron to carbon ratios but also the observed relationship between iron to carbon and dissolved iron concentrations. This supports using a nutrient-dependent "frugal phytoplankton" approach that has been proposed previously (Galbraith & Martiny, 2015).

The link between iron and carbon via phytoplankton Fe:C uptake has first order impacts on global nutrient cycling. When Fe:C ratios are fixed, surface nutrient concentrations are

immediately impacted, particularly in regions where atmospheric iron deposition rates are low, i.e. the Pacific HNLC region. This response is sensitive to the fixed value chosen, and results in significant increases or decreases in the areal extent of these regions. This leads to downstream effects on global water column denitrification, as reductions in the POC export in the nearby oxygen minimum zones is reduced when the iron supply is not able to maintain phytoplankton growth at the chosen fixed values. The flexibility of phytoplankton variable iron quotas is key to them maintaining productivity in regions of low deposition as previously mentioned, but also when that deposition changes. When only dust sourced iron is used to force the model, global NPP and POC export are reduced by 3% and 4% respectively when fixed stoichiometry is used. However, when variable stoichiometry is used, NPP and POC export increase by 0.2% and decrease by 1% respectively, showing that phytoplankton are able to acclimate according to changes in atmospheric deposition rates. However, this only dampens the biogeochemical response and there are limits to this acclimation as shown by the reductions in NPP and POC export when only pyrogenic sourced iron is used in both the variable and fixed scenarios.

Future changes in atmospheric iron deposition under different climate scenarios are still highly uncertain (Hamilton, Moore, et al., 2020; Mahowald et al., 2009, 2011). It is necessary to include pyrogenic-sources of iron in models of atmospheric iron deposition as this provides the primary iron source to remote ocean regions that are not as influenced by sedimentary or mineral dust iron sources. This includes the equatorial Pacific, where we see some of the greatest impacts on carbon and nutrient cycling under different deposition scenarios. In order to make reliable estimates of the interactions between the marine ecosystem and future changes in climate, pyrognic iron is key to accurately representing the marine nitrogen cycle in particular. Not accounting for this source could result in underestimates of global ocean nitrogen fixation and water column denitrification, which are integral to the global ocean fixed nitrogen inventory, and therefore carbon cycling in a primarily nitrogen limited ocean. Large shifts in the pyrogenic-sourced aerosols are likely in the future, responding to changes in wildfire activity and anthropogenic fossil fuel combustion patterns (Hamilton et al., 2022; Liu et al., 2022; Mahowald et al., 2009). It is therefore necessary to accurately account for pyrogenic-sourced iron as a key portion of biologically available iron in order to reliably model changes in the global carbon and nitrogen cycles under a changing climate.

Acknowledgments

The authors wish to thank the scientists and supporters of the GEOTRACES program, which provided support for the field observations used here. J.K.M. and N.A.W. acknowledge support from the U.S. Department of Energy, Biological and Environmental Research Division, Earth System Modeling Program grants DE-SC0016539 and DE-SC0022177. B.S.T. acknowledges support from NSF OCE-1829819 and OCE-2023237. D.S.H. and N.M.M. acknowledge support from DOE DE-SC0021302.

Open Research

The simulations used in this manuscript will be made available as .nc output files, while the compilation of phytoplankton iron to carbon observations will be made available as a .csv file in via Dryad.

References

Abraham, E. R., Law, C. S., Boyd, P. W., Lavender, S. J., Maldonado, M. T., & Bowie, A. R. (2000). Importance of stirring in the development of an iron-fertilized phytoplankton bloom. *Nature*, *407*(6805), 727–730.

Anderson, R. F. (2020). GEOTRACES: Accelerating Research on the Marine Biogeochemical Cycles of Trace Elements and Their Isotopes. *Annual Review of Marine Science*, *12*, 49–85.

Archer, D. E., & Johnson, K. (2000). A model of the iron cycle in the ocean. *Global Biogeochemical Cycles*, *14*(1), 269–279.

Berman-Frank, I., Cullen, J. T., Shaked, Y., Sherrell, R. M., & Falkowski, P. G. (2001). Iron

availability, cellular iron quotas, and nitrogen fixation in Trichodesmium. *Limnology and Oceanography*, *46*(6), 1249–1260.

Bopp, L., Kohfeld, K. E., Le Quéré, C., & Aumont, O. (2003). Dust impact on marine biota and atmospheric CO2during glacial periods. *Paleoceanography*, *18*(2). https://doi.org/10.1029/2002pa000810

Boyd, P. W., Jickells, T., Law, C. S., Blain, S., Boyle, E. A., Buesseler, K. O., et al. (2007). Mesoscale iron enrichment experiments 1993-2005: synthesis and future directions. *Science*, *315*(5812), 612–617.

Bruland, K. W., Donat, J. R., & Hutchins, D. A. (1991). Interactive influences of bioactive trace metals on biological production in oceanic waters. *Limnology and Oceanography*, *36*, 1555–1577.

Buchanan, P. J., Matear, R. J., Chase, Z., Phipps, S. J., & Bindoff, N. L. (2018). Dynamic Biological Functioning Important for Simulating and Stabilizing Ocean Biogeochemistry. *Global Biogeochemical Cycles*, *32*(4), 565–593.

Buesseler, K. O. (1998). The decoupling of production and particulate export in the surface ocean. *Global Biogeochemical Cycles*, *12*(2), 297–310.

Conway, T. M., Hamilton, D. S., Shelley, R. U., Aguilar-Islas, A. M., Landing, W. M., Mahowald, N. M., & John, S. G. (2019). Tracing and constraining anthropogenic aerosol iron fluxes to the North Atlantic Ocean using iron isotopes. *Nature Communications*, *10*(1), 2628.

Fung, I. Y., Meyn, S. K., Tegen, I., Doney, S. C., John, J. G., & Bishop, J. K. B. (2000). Iron supply and demand in the upper ocean. *Global Biogeochemical Cycles*, *14*(1), 281–295.

Galbraith, E. D., & Martiny, A. C. (2015). A simple nutrient-dependence mechanism for

predicting the stoichiometry of marine ecosystems. *Proceedings of the National Academy of Sciences of the United States of America*, *112*(27), 8199–8204.

Garcia, H., Weathers, K., Paver, C., Smolyar, I., Boyer, T., Locarnini, M., et al. (2019). World Ocean Atlas 2018. Vol. 4: Dissolved Inorganic Nutrients (phosphate, nitrate and nitrate+nitrite, silicate). *NOAA Atlas NESDIS 84*, 35pp.

Hamilton, D. S., Moore, J. K., Arneth, A., Bond, T. C., Carslaw, K. S., Hantson, S., et al. (2020). Impact of changes to the atmospheric soluble iron deposition flux on ocean biogeochemical cycles in the anthropocene. *Global Biogeochemical Cycles*, *34*(3), e2019GB006448.

Hamilton, D. S., Scanza, R. A., Rathod, S. D., Bond, T. C., Kok, J. F., Li, L., et al. (2020). Recent (1980 to 2015) trends and variability in daily-to-interannual soluble iron deposition from dust, fire, and anthropogenic sources. *Geophysical Research Letters*, *47*(17). https://doi.org/10.1029/2020gl089688

Hamilton, D. S., Perron, M. M. G., Bond, T. C., Bowie, A. R., Buchholz, R. R., Guieu, C., et al. (2022). Earth, Wind, Fire, and Pollution: Aerosol Nutrient Sources and Impacts on Ocean Biogeochemistry. *Annual Review of Marine Science*, *14*, 303–330.

Hopkinson, B. M., Seegers, B., Hatta, M., Measures, C. I., Greg Mitchell, B., & Barbeau, K. A. (2013). Planktonic C:Fe ratios and carrying capacity in the southern Drake Passage. *Deep-Sea Research. Part II, Topical Studies in Oceanography*, *90*, 102–111.

Ho, T.-Y., Quigg, A., Finkel, Z. V., Milligan, A. J., Wyman, K., Falkowski, P. G., & Morel, F. M. M. (2003). The elemental composition of some marine phytoplankton. *Journal of Phycology*, *39*(6), 1145–1159.

Howard, J. B., & Rees, D. C. (1996). Structural Basis of Biological Nitrogen Fixation. *Chemical Reviews*, *96*(7), 2965–2982.

527 Hudson, R. J. M., & Morel, F. M. M. (1990). Iron transport in marine phytoplankton: Kinetics of
528 cellular and medium coordination reactions. *Limnology and Oceanography*, *35*(5), 1002–
529 1020.
530 Ito, A., Myriokefalitakis, S., Kanakidou, M., Mahowald, N. M., Scanza, R. A., Hamilton, D. S.,
531 et al. (2019). Pyrogenic iron: The missing link to high iron solubility in aerosols. *Science*
532 *Advances*, *5*(5), eaau7671.
533 Ito, A., Ye, Y., Yamamoto, A., Watanabe, M., & Aita, M. N. (2020). Responses of ocean
534 biogeochemistry to atmospheric supply of lithogenic and pyrogenic iron-containing
535 aerosols. *Geological Magazine*, *157*(5), 741–756.
536 Jickells, T. D., & Spokes, L. J. (2001). Atmospheric iron inputs to the oceans. In *The*
537 *Biogeochemistry of Iron in Seawater* (Vol. SCOR/IUPAC Series, pp. 85–121). Wiley.
538 King, A. L., Sañudo-Wilhelmy, S. A., Boyd, P. W., Twining, B. S., Wilhelm, S. W., Breene, C.,
539 et al. (2012). A comparison of biogenic iron quotas during a diatom spring bloom using
540 multiple approaches. *Biogeosciences* , *9*(2), 667–687.
541 Krishnamurthy, A., Moore, J. K., Mahowald, N., Luo, C., & Zender, C. S. (2010). Impacts of
542 atmospheric nutrient inputs on marine biogeochemistry. *Journal of Geophysical Research*,
543 *115*(G1). https://doi.org/10.1029/2009jg001115
544 Kwiatkowski, L., Aumont, O., Bopp, L., & Ciais, P. (2018). The Impact of Variable
545 Phytoplankton Stoichiometry on Projections of Primary Production, Food Quality, and
546 Carbon Uptake in the Global Ocean. *Global Biogeochemical Cycles*, *32*(4), 516–528.
547 Lamb, K. D., Matsui, H., Katich, J. M., Perring, A. E., Spackman, J. R., Weinzierl, B., et al.
548 (2021). Global-scale constraints on light-absorbing anthropogenic iron oxide aerosols. *Npj*
549 *Climate and Atmospheric Science*, *4*(1), 1–12.

Lefèvre, N., & Watson, A. J. (1999). Modeling the geochemical cycle of iron in the oceans and its impact on atmospheric CO2concentrations. *Global Biogeochemical Cycles*, *13*(3), 727–736.

Liu, M., Matsui, H., Hamilton, D. S., Lamb, K. D., Rathod, S. D., Schwarz, J. P., & Mahowald, N. M. (2022). The underappreciated role of anthropogenic sources in atmospheric soluble iron flux to the Southern Ocean. *Npj Climate and Atmospheric Science*, *5*(1), 1–9.

Long, M. C., Moore, J. K., Lindsay, K., Levy, M., Doney, S. C., Luo, J. Y., et al. (2021). Simulations With the Marine Biogeochemistry Library (MARBL). *Journal of Advances in Modeling Earth Systems; Washington*, *13*(12). https://doi.org/10.1029/2021MS002647

Mahowald, N. M., Engelstaedter, S., Luo, C., Sealy, A., Artaxo, P., Benitez-Nelson, C., et al. (2009). Atmospheric iron deposition: global distribution, variability, and human perturbations. *Annual Review of Marine Science*, *1*, 245–278.

Mahowald, N. M., Lindsay, K., Rothenberg, D., Doney, S. C., Moore, J. K., Thornton, P., et al. (2011). Desert dust and anthropogenic aerosol interactions in the Community Climate System Model coupled-carbon-climate model. *Biogeosciences* , *8*(2), 387–414.

Maldonado, M. T., & Price, N. M. (1999). Utilization of iron bound to strong organic ligands by plankton communities in the subarctic Pacific Ocean. *Deep-Sea Research II*, *46*, 2447.

Marchetti, A., & Maldonado, M. T. (2016). Iron. In M. Borowitzka, J. Beardall, & J. Ravel (Eds.), *The physiology of Microalgae* (Vol. 6, pp. 233–279). Springer, Cham.

Martin, J. H., & Knauer, G. A. (1973). The elemental composition of plankton. *Geochimica et Cosmochimica Acta*, *37*(7), 1639–1653.

Matsui, H., Mahowald, N. M., Moteki, N., Hamilton, D. S., Ohata, S., Yoshida, A., et al. (2018). Anthropogenic combustion iron as a complex climate forcer. *Nature Communications*, *9*(1),

1593.

McKay, R. M. L., Wilhelm, S. W., Hall, J., Hutchins, D. A., Al-Rshaidat, M. M. D., Mioni, C. E., et al. (2005). Impact of phytoplankton on the biogeochemical cycling of iron in subantarctic waters southeast of New Zealand during FeCycle: PHYTOPLANKTON AND THE BIOGEOCHEMICAL CYCLING OF IRON. *Global Biogeochemical Cycles*, *19*(4). https://doi.org/10.1029/2005GB002482

Moore, C. M., Mills, M. M., Arrigo, K. R., Berman-Frank, I., Bopp, L., Boyd, P. W., et al. (2013). Processes and patterns of oceanic nutrient limitation. *Nature Geoscience*, *6*(9), 701–710.

Moore, J. K., & Braucher, O. (2008). Sedimentary and mineral dust sources of dissolved iron to the world ocean. *Biogeosciences* , *5*(3), 631–656.

Moore, J. K., Doney, S. C., Glover, D. M., & Fung, I. Y. (2002). Iron cycling and nutrient-limitation patterns in surface waters of the World Ocean. *Deep-Sea Research. Part II, Topical Studies in Oceanography*, *49*, 463–507.

Moore, J. K., Doney, S. C., & Lindsay, K. (2004). Upper ocean ecosystem dynamics and iron cycling in a global three-dimensional model. *Global Biogeochemical Cycles*, *18*(4). Retrieved from https://agupubs.onlinelibrary.wiley.com/doi/abs/10.1029/2004GB002220

Morel, F. M. M., Hudson, R. J. M., & Price, N. M. (1991). Limitation of productivity by trace metals in the sea. *Limnology and Oceanography*, *36*(8), 1742–1755.

Moreno, A. R., Hagstrom, G. I., Primeau, F. W., Levin, S. A., & Martiny, A. C. (2018). Marine phytoplankton stoichiometry mediates nonlinear interactions between nutrient supply, temperature, and atmospheric CO2. *Biogeosciences* , *15*(9). Retrieved from https://www.osti.gov/biblio/1503299

596 Myriokefalitakis, S., Ito, A., Kanakidou, M., Nenes, A., Krol, M. C., Mahowald, N. M., et al.
597 (2018). Reviews and syntheses: the GESAMP atmospheric iron deposition model
598 intercomparison study. *Biogeosciences* , *15*(21), 6659–6684.
599 Redfield, A. C., Ketchum, B. C., & Richards, F. A. (1963). The influence of organisms on the
600 composition of sea water. In N. Hill (Ed.), *The Sea* (Vol. 2, pp. 26–77). Hoboken, N. J.:
601 Wiley Intersci.
602 Sañudo-Wilhelmy, S. A., Kustka, A. B., Gobler, C. J., Hutchins, D. A., Yang, M., Lwiza, K., et
603 al. (2001). Phosphorus limitation of nitrogen fixation by Trichodesmium in the central
604 Atlantic Ocean. *Nature*, *411*(6833), 66–69.
605 Sarthou, G., Vincent, D., Christaki, U., Obernosterer, I., Timmermans, K. R., & Brussaard, C. P.
606 D. (2008). The fate of biogenic iron during a phytoplankton bloom induced by natural
607 fertilisation: Impact of copepod grazing. *Deep-Sea Research. Part II, Topical Studies in*
608 *Oceanography*, *55*(5), 734–751.
609 Schmidt, M. A., & Hutchins, D. A. (1999). Size-fractionated biological iron and carbon uptake
610 along a coastal to off shore transect in the NE Pacific. *Deep-Sea Research II*, *46*, 2487.
611 Schneider, B., Engel, A., & Schlitzer, R. (2004). Effects of depth-and CO2-dependent C: N
612 ratios of particulate organic matter (POM) on the marine carbon cycle. *Global*
613 *Biogeochemical Cycles*, *18*(2). Retrieved from
614 https://agupubs.onlinelibrary.wiley.com/doi/abs/10.1029/2003GB002184
615 Sedwick, P. N., Sholkovitz, E. R., & Church, T. M. (2007). Impact of anthropogenic combustion
616 emissions on the fractional solubility of aerosol iron: Evidence from the Sargasso Sea.
617 *Geochemistry, Geophysics, Geosystems*, *8*(10). https://doi.org/10.1029/2007gc001586
618 Séférian, R., Berthet, S., Yool, A., Palmiéri, J., Bopp, L., Tagliabue, A., et al. (2020). Tracking

619 Improvement in Simulated Marine Biogeochemistry Between CMIP5 and CMIP6. *Current*
620 *Climate Change Reports*, 1–25.
621 Sunda, W. G., & Huntsman, S. A. (1995). Iron uptake and growth limitation in oceanic and
622 coastal phytoplankton. *Marine Chemistry*, *50*(1), 189–206.
623 Sunda, W. G., Swift, D. G., & Huntsman, S. A. (1991). Low iron requirement for growth in
624 oceanic phytoplankton. *Nature*, *351*(6321), 55–57.
625 Tagliabue, A., Mtshali, T., Aumont, O., Bowie, A. R., Klunder, M. B., Roychoudhury, A. N., &
626 Swart, S. (2012). A global compilation of dissolved iron measurements: focus on
627 distributions and processes in the Southern Ocean. *Biogeosciences* , *9*(6), 2333–2349.
628 Tagliabue, A., Aumont, O., DeAth, R., Dunne, J. P., Dutkiewicz, S., Galbraith, E., et al. (2016).
629 How well do global ocean biogeochemistry models simulate dissolved iron distributions?
630 *Global Biogeochemical Cycles*, *30*(2), 149–174.
631 Tagliabue, A., Bowie, A. R., Boyd, P. W., Buck, K. N., Johnson, K. S., & Saito, M. A. (2017).
632 The integral role of iron in ocean biogeochemistry. *Nature*, *543*(7643), 51–59.
633 Tagliabue, A., Barrier, N., Du Pontavice, H., Kwiatkowski, L., Aumont, O., Bopp, L., et al.
634 (2020). An iron cycle cascade governs the response of equatorial Pacific ecosystems to
635 climate change. *Global Change Biology*. https://doi.org/10.1111/gcb.15316
636 Tanioka, T., & Matsumoto, K. (2017). Buffering of ocean export production by flexible
637 elemental stoichiometry of particulate organic matter. *Global Biogeochemical Cycles*,
638 *31*(10), 1528–1542.
639 Tovar-Sanchez, A., Sañudo-Wilhelmy, S. A., Garcia-Vargas, M., Weaver, R. S., Popels, L. C., &
640 Hutchins, D. A. (2003). A trace metal clean reagent to remove surface-bound iron from
641 marine phytoplankton. *Marine Chemistry*, *82*(1), 91–99.

642 Twining, B. S., Baines, S. B., Fisher, N. S., Maser, J., Vogt, S., Jacobsen, C., et al. (2003).
643 Quantifying trace elements in individual aquatic protist cells with a synchrotron X-ray
644 fluorescence microprobe. *Analytical Chemistry*, *75*(15), 3806–3816.
645 Twining, B. S., Baines, S. B., Fisher, N. S., & Landry, M. R. (2004). Cellular iron contents of
646 plankton during the Southern Ocean Iron Experiment (SOFeX). *Deep Sea Research Part I:*
647 *Oceanographic Research Papers*, *51*(12), 1827–1850.
648 Twining, B. S., Nuñez-Milland, D., Vogt, S., Johnson, R. S., & Sedwick, P. N. (2010).
649 Variations in Synechococcus cell quotas of phosphorus, sulfur, manganese, iron, nickel, and
650 zinc within mesoscale eddies in the Sargasso Sea. *Limnology and Oceanography*, *55*(2),
651 492–506.
652 Twining, B. S., Baines, S. B., Bozard, J. B., Vogt, S., Walker, E. A., & Nelson, D. M. (2011).
653 Metal quotas of plankton in the equatorial Pacific Ocean. *Deep-Sea Research. Part II,*
654 *Topical Studies in Oceanography*, *58*(3), 325–341.
655 Twining, B. S., Rauschenberg, S., Morton, P. L., & Vogt, S. (2015). Metal contents of
656 phytoplankton and labile particulate material in the North Atlantic Ocean. *Progress in*
657 *Oceanography*, *137*, 261–283.
658 Twining, B. S., Rauschenberg, S., Baer, S. E., Lomas, M. W., Martiny, A. C., & Antipova, O.
659 (2019). A nutrient limitation mosaic in the eastern tropical Indian Ocean. *Deep-Sea*
660 *Research. Part II, Topical Studies in Oceanography*, *166*, 125–140.
661 Twining, B. S., Antipova, O., Chappell, P. D., Cohen, N. R., Jacquot, J. E., Mann, E. L., et al.
662 (2021). Taxonomic and nutrient controls on phytoplankton iron quotas in the ocean.
663 *Limnology and Oceanography Letters*, *6*(2), 96–106.
664 Ustick, L. J., Larkin, A. A., Garcia, C. A., Garcia, N. S., Brock, M. L., Lee, J. A., et al. (2021).

665 Metagenomic analysis reveals global-scale patterns of ocean nutrient limitation. *Science*,
666 *372*(6539), 287–291.
667 Volk, T., & Hoffert, M. I. (1985). Ocean carbon pumps: Analysis of relative strengths and
668 efficiencies in ocean-driven atmospheric CO2 changes. *The Carbon Cycle and Atmospheric*
669 *CO2: Natural Variations Archean to Present*, *32*, 99–110.
670 Wang, W.-L., Moore, J. K., Martiny, A. C., & Primeau, F. W. (2019). Convergent estimates of
671 marine nitrogen fixation. *Nature*, *566*(7743), 205–211.
672 Weber, T., & Deutsch, C. (2012). Oceanic nitrogen reservoir regulated by plankton diversity and
673 ocean circulation. *Nature*, *489*(7416), 419–422.
674 Wu, J., & Boyle, E. (2002). Iron in the Sargasso Sea: Implications for the processes controlling
675 dissolved Fe distribution in the ocean. *Global Biogeochemical Cycles*, *16*(4), 33–1–33–8.